

Wilcoxon Nonparametric CFAR Scheme for Ship Detection in SAR Image

Xiangwei Meng

Department of Electrical and Electronic Engineering, Yantai Nanshan University, Yantai 265713, China
E-mail: (mengxw163@sohu.com)

Abstract: The parametric constant false alarm rate (CFAR) detection algorithms which are based on various statistical distributions, such as Gaussian, Gamma, Weibull, log-normal, G^0 distribution, alpha-stable distribution, etc, are most widely used to detect the ship targets in SAR image at present. However, the clutter background in SAR images is complicated and variable. When the actual clutter background deviates from the assumed statistical distribution, the performance of the parametric CFAR detector will deteriorate. In addition to the parametric CFAR schemes, there is another class of nonparametric CFAR detectors which can maintain a constant false alarm rate for the target detection without the assumption of a known clutter distribution. In this work, the Wilcoxon nonparametric CFAR scheme for ship detection in SAR image is proposed and analyzed, and a closed form of the false alarm rate for the Wilcoxon nonparametric detector to determine the decision threshold is presented. By comparison with several typical parametric CFAR schemes on Radarsat-2, ICEYE-X6 and Gaofen-3 SAR images, the robustness of the Wilcoxon nonparametric detector to maintain a good false alarm performance in different detection backgrounds is revealed, and its detection performance for the weak ship in rough sea surface is improved to some extent. Moreover, the Wilcoxon nonparametric detector can suppress the false alarms resulting from the sidelobes at some degree and its detection speed is fast.

Keywords: constant false alarm rate (CFAR), nonparametric detection, nonGaussian distribution, synthetic aperture radar (SAR), Wilcoxon detector

I. INTRODUCTION

Synthetic aperture radar (SAR) has been widely used for earth remote sensing for many years. It provides high resolution images independent from daylight, cloud coverage and weather conditions. The ship detection in SAR images is an important application of SAR remote sensing and attracts more interest of experts engaged in this field. It can be used for ship traffic monitoring, port security, anti-piracy and military applications. Among many methods to detect ship target in SAR images, the constant false alarm rate (CFAR) scheme is the most extensively and effectively used technique. The famous one is the two-parameter CFAR detector^[1], which uses the estimated mean and standard deviation of the clutter samples within a square band window centered around the pixel under test to set an adaptive threshold. The two-parameter CFAR detector can maintain a constant false alarm rate with the assumption of Gaussian background.

When the radar resolution increases, the distribution of the SAR clutter deviates from the Gaussian assumption

and shows a long tail of the distribution. In order to improve the performance for the ship detection in SAR images, various statistical distributions were used to model the SAR clutter backgrounds^[2-11], such as K, the alpha-stable distribution, G^0 , log-normal, Gamma, Rayleigh, Rayleigh mixtures distribution, etc. In [2], the simulated annealing method was used to segment the high resolution SAR image into different regions with homogeneous characteristics, and the CA-CFAR based on the K distribution was performed inside each homogeneous region. In [3], the K-means program was used to segment a SAR image into N sub-images and the CFAR detection based on alpha-stable distribution was carried out. In [4], an adaptive and fast CFAR algorithm based on G^0 distribution for the ships detection in SAR image was proposed. In [5], the log-normal distribution was used to model the clutter background in SAR images and a multilayer CFAR detection for ship target in SAR images was proposed, which detects and eliminates the target pixels repeatedly. In order to reduce the influence of the multiple targets on the estimation of the background statistics, the truncated statistics (TS) CFAR method^[6] based on Gamma distribution for ship detection in single-look intensity and multi-look intensity SAR data was proposed. In [7], a novel and fast target detection approach called as RmSAT-CFAR for SAR images was presented, which uses Rayleigh mixtures for the clutter modeling. An outliers-robust CFAR detector which aims at elevating the detection performance in multiple targets situation is proposed in [8], which assumes a Gaussian distribution for the sea clutter in SAR image. In [9], a robust constant false alarm rate detector based on censored harmonic averaging (CHA-CFARD) is proposed for dense interfering targets situation, and its effectiveness is verified by the ship detection in TerraSAR-X image. In [10], a robust CFAR detector based on bilateral-trimmed-statistics called as the BTS-RCFAR for the ship detection in SAR image is proposed, which uses the log-normal distribution to fit the sea clutter in SAR image. In [11], an automatic identification system (AIS) data aided Rayleigh constant false alarm rate (AIS-RCFAR) ship detection algorithm was proposed. It uses the Rayleigh distribution to model the clutter in SAR image and design a clutter trimming method with an adaptive-trimming-depth aided by AIS data to effectively eliminate the high-intensity outliers in the local background window.

The CFAR techniques for the detection of radar targets can be divided into two broad categories: the parametric CFAR and the nonparametric or distribution-free detection methods, depending on whether or not a known distribution form is assumed for the clutter background.

As for the target detection in SAR image, the majority of the existing detection methods belong to the parametric CFAR type. If the actual clutter distribution departs from the assumed form, the detection performance of the parametric CFAR detector may degrade substantially, whereas the nonparametric CFAR procedure exhibits its advantage that it can maintain a constant false alarm rate in spite of changes of the underlying data distribution. Therefore, the primary motivation of this work is to propose a new path to perform the ship target detection in SAR image, that is, by application of the well-known Wilcoxon nonparametric detector to the ship target detection in SAR image. In [12], the Wilcoxon two-sample nonparametric detector was applied to the low-resolution radar target detection, which is usually termed as the rank sum (RS) nonparametric detector in the literature. The generalized sign test detector^[13] was proposed at the same time, and it has the same form as the RS nonparametric detector. A closed form expression of false alarm rate of the RS nonparametric detector in homogeneous background has been derived by Akimov (in Russian), and it was reported by M. Sekine and Y. H. Mao^[14]. The analytical expressions of the false alarm rate for the RS and rank quantization (RQ) nonparametric detector^[15] in nonhomogeneous background were derived in [16] and [17], respectively.

In this work, the Wilcoxon nonparametric method for the ship detection in SAR image is proposed and analyzed. The description of the Wilcoxon nonparametric method for the ship detection in SAR images is given in section II. The performance of Wilcoxon nonparametric method to detect the ships in Radarsat-2, ICEYE-X6 and Gaofen-3 SAR images is analyzed, and a comparison to the two-parameter CFAR, the Weibull CFAR and the most popular TS-CFAR is presented in section III. Finally, we summarize and discuss the results obtained.

II. THE DESCRIPTION OF THE WILCOXON DETECTOR FOR THE SHIP DETECTION IN SAR IMAGE

In a conventional CFAR system, target detection is commonly performed using the sliding widow technique. The data available in the reference window enter into an algorithm for the calculation of the decision threshold. For the ship detection in SAR images with the Wilcoxon nonparametric CFAR detector, a sketch of the two-dimensional sliding window is shown in Fig.1. As shown in the figure, the cells (pixels) under test are at the center of a defined local region, and the cells in the boundary stencil are the reference cells, and also the cells between the test cells and the reference cells are the guard cells. The guard area ensures that no target signal energy spill over into the reference cells. Let Y_1, \dots, Y_n denotes the reference cells in background region, whereas X_1, \dots, X_m represents the test cells to decide whether or not a target is present.

We assume that X_1, \dots, X_m and Y_1, \dots, Y_n are independent and identically distributed (IID) random samples with probability density function (PDF) $f(x)$ and $g(x)$, respectively. Under the null hypothesis H_0 , the test samples X_1, \dots, X_m and the reference samples Y_1, \dots, Y_n are IID and have a same distribution. We also assume that two samples are drawn from continuous distributions, so that the possibility $X_i = Y_j$ for some i and j need not to be considered. Setting $X_{m+j} = Y_j$, $j = 1, \dots, n$, and $N = m + n$, we obtain a combined samples set X_1, \dots, X_N . The combined samples X_1, \dots, X_N are first rank-ordered according to increasing magnitude. The sequence thus obtained is

$$X_{(1)} \leq X_{(2)} \leq \dots \leq X_{(N)} \quad (1)$$

The sequence given in (1) is called as order statistic. The indices in parentheses indicate the rank-order number. Let R_i ($i = 1, \dots, N$) denote the rank of the observation X_i in the ordered sequence (1). We observe that R_1, \dots, R_m are the ranks corresponding to the test samples X_1, \dots, X_m in the combined samples X_1, \dots, X_N .

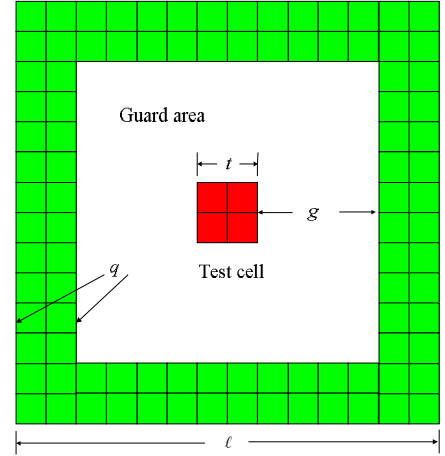


Fig.1. The sliding window of the Wilcoxon nonparametric CFAR detector.

In order to decide whether or not a radar target exists in the test cells, we apply the Wilcoxon nonparametric CFAR detector to this situation. The Wilcoxon test statistic is in the form of

$$S_{m,n} = \sum_{i=1}^m R_i \quad (2)$$

If $S_{m,n}$ exceeds a decision threshold T_W ($S_{m,n} \geq T_W$), a target is declared to be present in the test cells. On the other hand, if it is less than T_W ($S_{m,n} < T_W$), the target is absent. The decision threshold T_W is chosen to yield the desired false alarm probability P_{fa} .

Theorem 1^[18]: Let $S_{m,n}$ be the two-sample Wilcoxon test statistic, for the samples X_1, \dots, X_m and Y_1, \dots, Y_n . Under the null hypothesis H_0 , the probability of the

Wilcoxon test statistic taking $S_{m,n} = k$ is

$$P\{S_{m,n} = k\} = \frac{\pi_{m,n}(k)}{\binom{N}{m}} \quad (3)$$

for $k = \frac{1}{2}m(m+1), \frac{1}{2}m(m+1)+1, \dots, \frac{m(m+2n+1)}{2}$,

where $\pi_{m,n}(k)$ satisfy the recurrence formula

$$\pi_{m,n}(k) = \pi_{m,n-1}(k) + \pi_{m-1,n}(k-m-n) \quad (4)$$

with the initial and boundary conditions:

$$\pi_{i,0}\left(\frac{1}{2}i(i+1)\right) = 1; \quad (5)$$

$$\pi_{i,0}(k) = 0, \text{ for } k \neq \frac{1}{2}i(i+1), \quad i = 1, \dots, m; \quad (6)$$

$$\pi_{0,j}(0) = 1; \quad (7)$$

$$\pi_{0,j}(k) = 0, \text{ for } k \neq 0, \quad j = 1, \dots, n; \quad (8)$$

The notation $\pi_{m,n}(k)$ in (3) is the number of distinguishable arrangements of samples X_1, \dots, X_m and Y_1, \dots, Y_n , regardless of their indices, in $X_{(1)}, \dots, X_{(N)}$,

such that $S_{m,n} = \sum_{i=1}^m R_i = k$.

For readability, the proof of the Theorem 1 in [18] is also cited here.

Proof:

Let us denote by $\pi_{m,n}(k)$ the number of arrangements of observations $\{X_i\}$ and $\{Y_j\}$, regardless of their indices, in $X_{(1)}, \dots, X_{(m+n)}$, such that $S_{m,n} = \sum_{i=1}^m R_i = k$.

Now, (3) is obvious, and (4) follows easily by discarding the observations $X_{(m+n)}$. Actually, if $X_{(m+n)}$ is some Y_j we get $S_{m,n-1} = k$, and if $X_{(m+n)}$ is some X_i , we get $S_{m-1,n} = k - m - n$.

Under the null hypothesis H_0 , if the Wilcoxon test statistic $S_{m,n}$ is greater than a decision threshold T_W , a false alarm occurs. Therefore, the false alarm probability of the Wilcoxon nonparametric CFAR scheme for the ship detection in SAR images is expressed as

$$P_{fa} = \sum_{k=T_W}^{m(m+2n+1)/2} P\{S_{m,n} = k\} = \sum_{k=T_W}^{m(m+2n+1)/2} \frac{\pi_{m,n}(k)}{\binom{N}{m}} \quad (9)$$

It can be observed that the derivation of the false alarm rate P_{fa} of the Wilcoxon nonparametric CFAR method for the ship detection in SAR images is irrelevant to the distribution of background clutter. Therefore, the Wilcoxon nonparametric CFAR scheme for the ship detection in SAR images can maintain a constant false alarm rate regardless of the distribution of clutter background. This is what we call the distribution-free property of a nonparametric CFAR detector.

Since the Mann-Whitney nonparametric detector is equivalent to the Wilcoxon scheme^[19] and it is easy to be implemented, we replace the Wilcoxon scheme by the Mann-Whitney detector in our analysis. The test statistic of the Mann-Whitney nonparametric detector is defined as

$$R_{MW} = \sum_{i=1}^m \sum_{j=1}^n u(x_i - y_j) \quad (10)$$

where the $u(t)$ is the unit step function,

$$u(t) = \begin{cases} 1 & t \geq 0 \\ 0 & t < 0 \end{cases}.$$

If the test statistic R_{WM} of the Mann-Whitney detector is greater than the decision threshold T_{MW} , a declaration about the presence of a target in the test window is made; otherwise, no target exist. The relationship between the test statistic of the Wilcoxon detector and that of the Mann-Whitney detector is

$$S_{m,n} = R_{MW} + \frac{1}{2}m(m+1).$$

The decision threshold T_{MW} of the Mann-Whitney nonparametric detector for a nominal/design false alarm rate P_{fa} can also be obtained with substitution of $T_{MW} = T_W - \frac{1}{2}m(m+1)$.

III. EXPERIMENTAL RESULTS AND PERFORMANCE ANALYSIS

The performance of the Wilcoxon nonparametric CFAR scheme for the ship detection in SAR image is verified by 3 SAR image scenes: the SAR ship detection in calm sea surface, the SAR ship detection in rough sea surface and the weak ship detection in rough SAR background. They are collected by Radarsat-2, ICEYE-X6 and Gaofen-3, respectively. The detection results of the Wilcoxon nonparametric CFAR detector for ships in 3 SAR scenes will be presented and analyzed in the following.

A. The SAR ship detection in calm sea surface.

1) The SAR Image #1 collected by Radarsat-2

The first SAR image data being examined here were acquired by the C-band Radarsat-2 with the standard mode on March 8, 2010, around a seaport near Tokyo, Japan. The polarization mode is HH. The acquired SAR image is shown in Fig.2. The SLC data cover a scene of about 20 km by 20 km, which corresponds to an image of size 16036×11955 . The azimuth and range resolution is 3m, respectively. In order to validate the detection performance of the Wilcoxon nonparametric detector, a slice marked by a white rectangular in Fig.2 is cut, which is the SAR image #1 shown in Fig.3. The SAR image #1 is of size 1001×901 and 4 ships are visible, and the extended sidelobes caused by the strong reflections of the ship body can be clearly observed. The sea surface in the SAR image is calm, but there exist some speckles in the background.



Fig.2. The SAR image was acquired by the C-band Radarsat-2 on March 8, 2010, around a seaport near Tokyo, Japan.

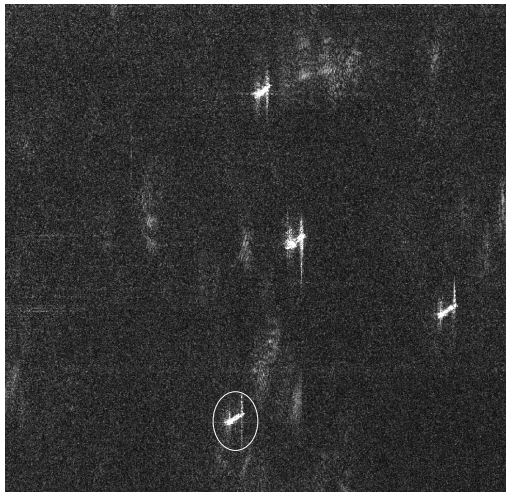


Fig.3. The SAR image #1 from Radarsat-2.

Although the Wilcoxon nonparametric detector can detect targets in nonGaussian background at a constant false alarm rate without assumption of known distribution, in order to make a comparison to other parametric CFAR schemes, a statistical distribution analysis for the SAR image data is necessary. In the design stage of a CFAR detection scheme, a relatively low nominal/design value of the false alarm rate for conventional radar is usually determined in a homogeneous background. Therefore, the pixels resulting from 4 targets should be discarded from the SAR image #1 firstly, with attempt to accurately model the clutter background. The statistical analysis of the SAR image #1 is given in Fig.4. The histogram of pixels of the clutter background in SAR image #1 is depicted in Fig.4, and the PDF curves of Gaussian, Weibull, K and Gamma distributions to fit the background clutter data are also included. It is noted that 2 cases of Gamma distribution are presented in Fig.4, one is that the shape parameter of Gamma distribution is estimated by

the maximum likelihood method, which is denoted by “Gamma”, and the other is that the shape parameter of Gamma distribution is replaced by the equivalent number of looks (ENL), which is represented by “Gamma-ENL”. It can be seen that the main body of the PDF of K distribution and that of Weibull distribution fit the histogram of the SAR image #1 relatively well, and the worst case is obtained by Gaussian distribution. The main body of the PDF of both Gamma distributions deviates from the histogram of the SAR image #1 to a certain extent.

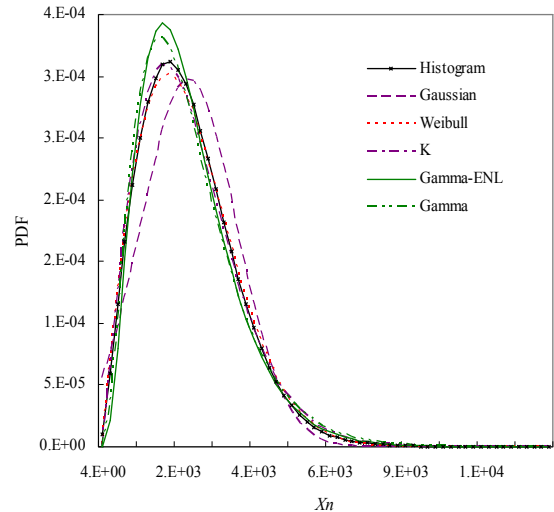


Fig.4. The analysis of statistical distribution on the SAR image #1.

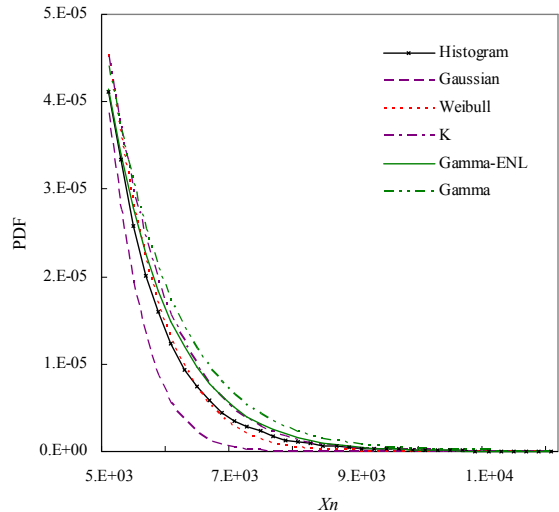


Fig.5. The tails of statistical distribution of the SAR image #1.

In fact, the tail of the PDF on the right side determines the false alarm performance of a CFAR detection scheme. In order to inspect the difference between the tails of the PDF of these distributions in detail, the tails of these distributions are illustrated in Fig.5 again. It can be seen that the tail of the Gaussian distribution significantly deviates from that of the histogram of the SAR image #1. As the grey value X_n becomes large, the tail of the Weibull crosses the histogram of the SAR image #1 and is slightly lower than it. The tail of the K distribution and that of the

Gamma distribution with ENL almost come together and are slightly higher than that of the histogram, whereas the tail of the Gamma distribution with maximum likelihood estimation is even higher than them. The shape parameter of the Gamma distribution with maximum likelihood estimation is 2.99, and the ENL to replace the actual shape parameter is 3.33. It can be seen that although these PDF curves of different statistical distribution approaches the histogram of the SAR image #1 at varying degrees, all of them can not coincide with it completely.

2) The performance analysis of the Wilcoxon nonparametric detector

The Wilcoxon detector takes a sliding window of size $\ell \times \ell = 68 \times 68$ and a width $g=30$ of guard area and a test window of size $t \times t=2 \times 2$. The ℓ , g and t is shown in Fig.1, respectively. In order to avoid the influence of the pixels under test on the background clutter estimation, the width of guard area is longer than the length of the largest ship in the SAR image. For the Wilcoxon nonparametric detector in our experiments, the boundary clutter samples of $q=3$ row/column in the sliding window form the reference samples to set the detection threshold, and the total number of the reference samples is 780.

In order to make a comparison with the parametric CFAR schemes, we consider the two-parameter CFAR and the Weibull CFAR^[20], and the most popular TS-CFAR^[6] at present as a reference. The two-parameter CFAR, the Weibull CFAR and the TS-CFAR operate in a conventional pixel by pixel detection approach. Only a single pixel in the test window is detected at a time, and the same width $g=30$ of the guard area is used for them. Since a number of 248 clutter samples in the reference window are sufficient for the maximum-likelihood estimation of distribution parameters, a single boundary row/column $q=1$ of clutter samples in the reference window are adopted for them. Here, a sliding window of size $\ell \times \ell = 63 \times 63$ is taken for the two-parameter CFAR, the Weibull CFAR and the TS-CFAR. The TS-CFAR scheme takes a truncation ratio^[6] at $R_t = 10\%$, and it uses the ENL to replace the actual shape parameter.

The detection result of the two-parameter CFAR is shown in Fig.6 (a), (b) and (c) for the design false alarm rate $P_{fa}=10^{-5}$, 10^{-6} and 10^{-7} , respectively. We utilize the maximum-likelihood estimation to obtain the mean and the variance of the background clutter, and then set the adaptive detection threshold. The detection result of the Weibull CFAR is shown in Fig.7 (a), (b) and (c) for the design false alarm rate $P_{fa}=10^{-3}$, 10^{-4} and 10^{-5} , respectively. We can find an interesting phenomenon that the detection result of the two-parameter CFAR at $P_{fa}=10^{-7}$ is similar to that of the Weibull CFAR at $P_{fa}=10^{-5}$. This is due to the fact that the two-parameter CFAR assumes a Gaussian distribution for the background clutter, whereas the actual clutter in the SAR image obeys a nonGaussian distribution with a long tail, so that a higher detection threshold for the

two-parameter CFAR at $P_{fa}=10^{-7}$ is required to achieve the similar detection effects of the Weibull CFAR at $P_{fa}=10^{-5}$. Therefore, the comparison of detection performance between the detectors with different assumed distributions under the same nominal/design false alarm rate P_{fa} is unfair. In [21], the false discovery rate (FDR) is controlled for a specific surveillance area, unlike the conventional CFAR scheme of controlling a nominal probability of false alarm P_{fa} . This motivates us to replace the nominal/design P_{fa} by the FDR for the performance comparison of different detectors for a specific SAR image. Actually, the FDR is often of more practical importance than the conventional nominal/design false alarm rate P_{fa} ^[21].

For the ship detection in a SAR image, the FDR is defined as the ratio of the number of false alarms to the total number of observations classified into the alternative hypotheses (H_1), that is

$$FDR = \frac{V}{V + S} \quad (11)$$

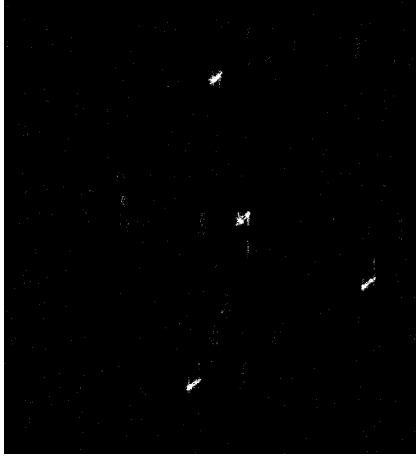
where V is the number of false alarms, S is the number of the true decisions about the presence of targets (declared H_1 when H_1 is true). For the calculation of V , an isolated bright spot in the detection image counts as 1 false alarm. In Fig.6 (a), (b) and Fig.7 (a), (b), the bright spots originating from the sea background and sidelobes are too many (false alarms), so that the FDR in these cases are not given. In Fig.6 and Fig.7, four ships are counted as $S=4$. The FDR for the two-parameter CFAR in Fig.6 (c) and that of the Weibull CFAR in Fig.7 (c) is $FDR \approx 0.94$ and $FDR \approx 0.92$, respectively.

The detection result of the TS-CFAR scheme with the truncation ratio $R_t = 10\%$ for the SAR image #1 at the design false alarm rate $P_{fa}=10^{-2}$, 10^{-3} and 10^{-4} is shown in Fig.8 (a), (b) and (c), respectively. Since the TS-CFAR assumes a Gamma distribution for the clutter background and the tail of Gamma distribution is slightly higher than that of the Weibull distribution, the TS-CFAR at $P_{fa}=10^{-4}$ gives the similar detection effects to that of the Weibull CFAR at $P_{fa}=10^{-5}$. However, most of false alarms of the TS-CFAR are caused by the sidelobes of the ship. This is different from the case of the two-parameter CFAR and the Weibull CFAR. Most of the false alarms of the two-parameter CFAR and the Weibull CFAR are resulted by the sea background clutter.

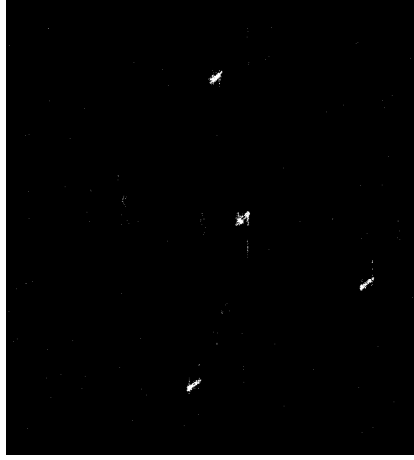
The detection result of the Wilcoxon nonparametric detector for the SAR image #1 at the design false alarm rate $P_{fa}=10^{-6}$, 10^{-7} and 10^{-8} is shown in Fig.9 (a), (b) and (c), respectively. It can be seen that the false alarm performance of the two-parameter CFAR in Fig.6(c), that of the Weibull CFAR in Fig.7(c), that of the TS-CFAR in Fig.8(c) and that of the Wilcoxon nonparametric detector in Fig.9(c) are similar, i.e., they have a similar FDR. It can also be observed that the Wilcoxon nonparametric detector can suppress the false alarms resulting from sidelobe of the ship body to some extent. This advantage of the Wilcoxon nonparametric detector is displayed in Fig.10

for the ship in the white circle in the SAR image #1. It can be seen that the sidelobes of the ship by the Wilcoxon nonparametric detector are suppressed evidently with comparison to the two-parameter CFAR, the Weibull

CFAR and the TS-CFAR algorithm. This lies in the fact that the Wilcoxon nonparametric detector takes a $t \times t=2 \times 2$ test window such that the wirelike sidelobes can be suppressed to some extent.



(a) $P_{fa}=10^{-5}$, FDR≈--

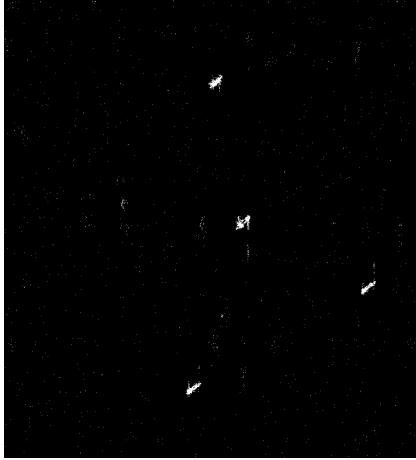


(b) $P_{fa}=10^{-6}$, FDR≈--

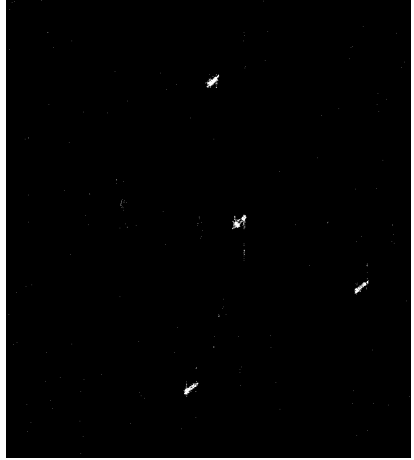


(c) $P_{fa}=10^{-7}$, FDR≈0.94

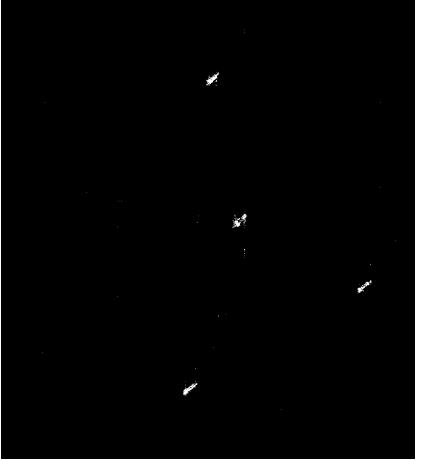
Fig.6. The detection results of the two-parameter CFAR on the SAR image #1.



(a) $P_{fa}=10^{-3}$, FDR≈--

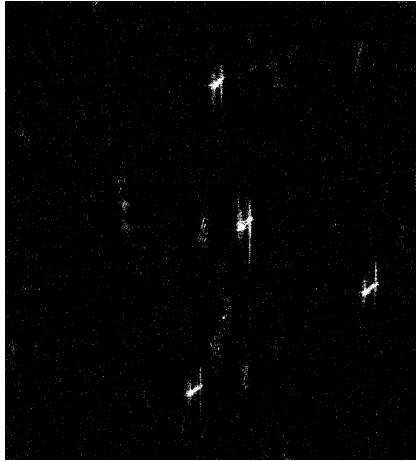


(b) $P_{fa}=10^{-4}$, FDR≈--

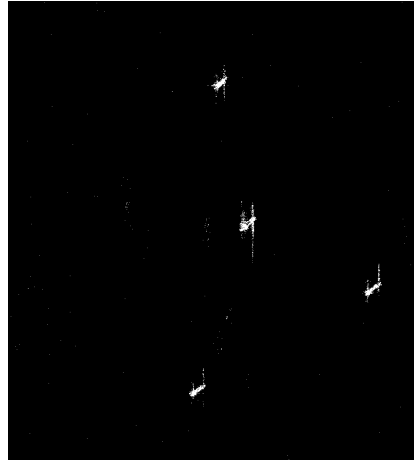


(c) $P_{fa}=10^{-5}$, FDR≈0.92

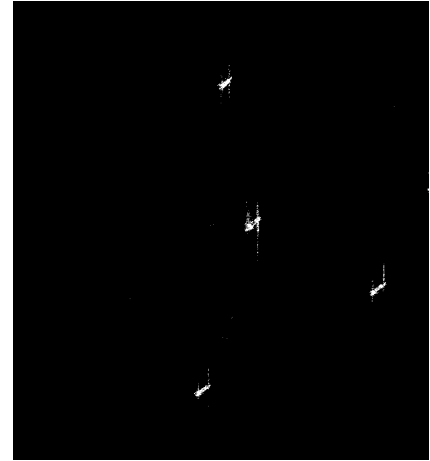
Fig.7. The detection results of the Weibull CFAR on the SAR image #1.



(a) $P_{fa}=10^{-2}$, FDR≈--

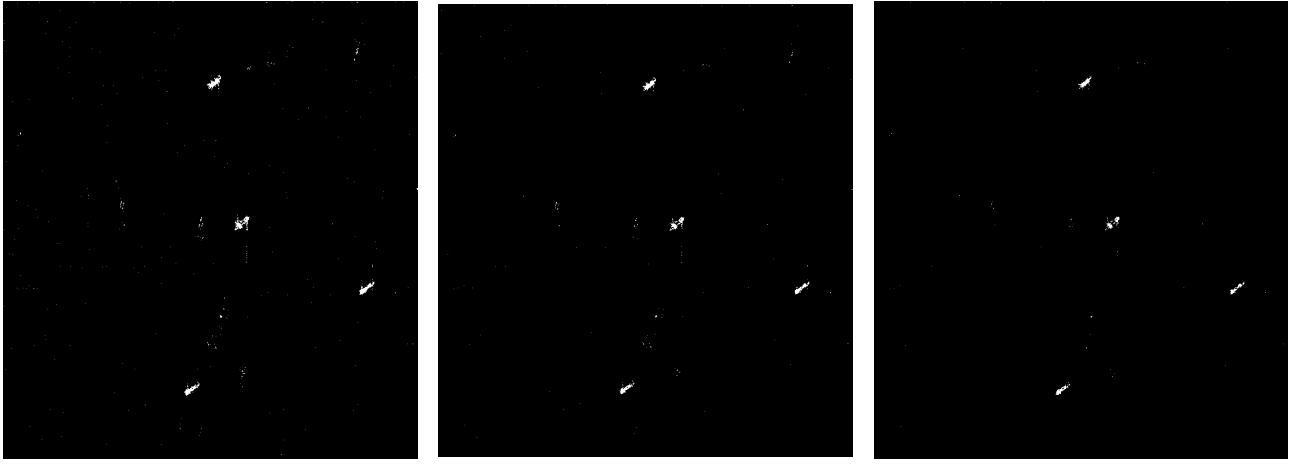


(b) $P_{fa}=10^{-3}$, FDR≈--



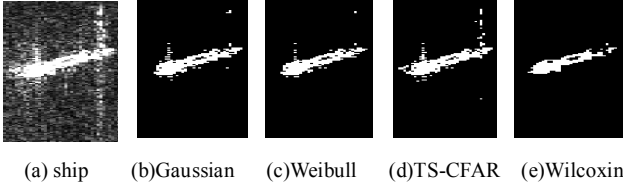
(c) $P_{fa}=10^{-4}$, FDR≈0.98

Fig.8. The detection results of the TS-CFAR scheme on the SAR image #1.



(a) $P_{fa}=10^{-6}$, FDR≈-- (b) $P_{fa}=10^{-7}$, FDR≈-- (c) $P_{fa}=10^{-8}$, FDR≈0.92

Fig.9. The detection results of the Wilcoxon nonparametric detector on the SAR image #1



(a) ship (b)Gaussian (c)Weibull (d)TS-CFAR (e)Wilcoxin

Fig.10. The detection effects of several detectors on the ship of the SAR image #1.

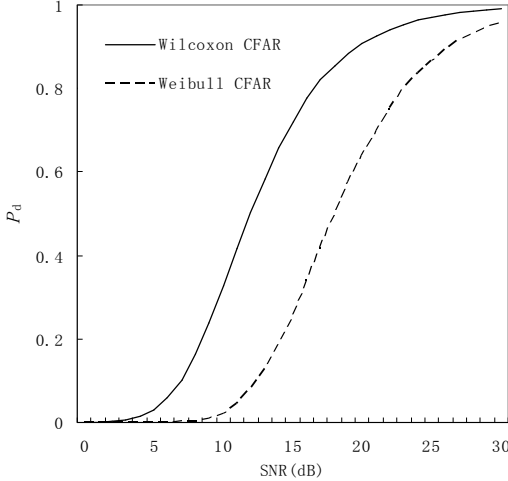


Fig.11. The detection performance of the Wilcoxon nonparametric detector.

Naturally, a question arises now. The false alarm rate of the Wilcoxon nonparametric detector is irrelative to the background clutter distribution. Why does the Wilcoxon nonparametric detector take a lower nominal false alarm rate $P_{fa}=10^{-8}$ to reach the similar FDR? The cause behind this phenomenon is that the Wilcoxon nonparametric detector takes 4 pixels in the test window to perform the ship detection in the SAR image, whereas the two-parameter CFAR and the Weibull CFAR take only a single pixel under test to accomplish this task. The speckles in the SAR image appear to be cotton-like and slice-like, thus they occupy a number of pixels. They will

be more possible to be detected as false alarms by the Wilcoxon nonparametric detector when the ship targets are detected.

In Fig.11, a comparison of the detection performance of the Wilcoxon nonparametric detector with 4 test pixels and 780 reference samples to that of the Weibull CFAR with a single pixel under test and 248 reference samples is made by Monte Carlo simulation, under the same nominal false alarm rate $P_{fa}=10^{-5}$. We assume that the background clutter follows the Weibull distribution and the intensity of the pixels of ship target obeys Swerling II fluctuation. In the simulation, the target plus the background clutter in the test cells add as vectors. It can be seen that the Wilcoxon nonparametric detector shows a better detection performance than the Weibull CFAR under the same nominal false alarm rate $P_{fa}=10^{-5}$. This means that while the pixels of the ship target are detected by the Wilcoxon nonparametric CFAR detector at a high detection probability, the speckles in the SAR image are also detected easily. Therefore, a higher detection threshold corresponding to a lower nominal false alarm rate is required by the Wilcoxon nonparametric detector to suppress the resulting false alarms in a specific SAR image scene.

3) The time cost of the Wilcoxon nonparametric detector

The time cost is an important aspect for the performance of CFAR detection scheme. It determines whether or not an algorithm can be successfully applied in practical application. The CFAR detection schemes examined in this work are implemented by MATLAB codes, running on a PC with an Intel Core i7 CPU of 3.0 GHz and 16 GB memory. The execution times of the two-parameter CFAR (denoted as TP-CFAR in the Table I), the Weibull CFAR, the TS-CFAR and the Wilcoxon nonparametric detector on the SAR image #1 are given in Table I, respectively. It's shown that the time cost of the Wilcoxon nonparametric detector on the SAR image #1 is the least among these CFAR schemes, and reduces more

than half of that of the two-parameter CFAR. The time cost of the TS-CFAR is the longest. This is due to the fact that the Wilcoxon nonparametric detector does not assume a known form for background distribution, thus it avoids the large and complicated computation on the parameters estimation for the parametric CFAR detectors.

TABLE I

The execution times of several CFAR detectors on the SAR image #1

| TP-CFAR | Weibull | TS-CFAR | Wilcoxon |
|---------|---------|---------|----------|
| 30.29s | 319.98s | 918.26s | 12.51s |

B. The SAR ship detection in rough sea surface.

1) The SAR Image #2 collected by ICEYE-X6

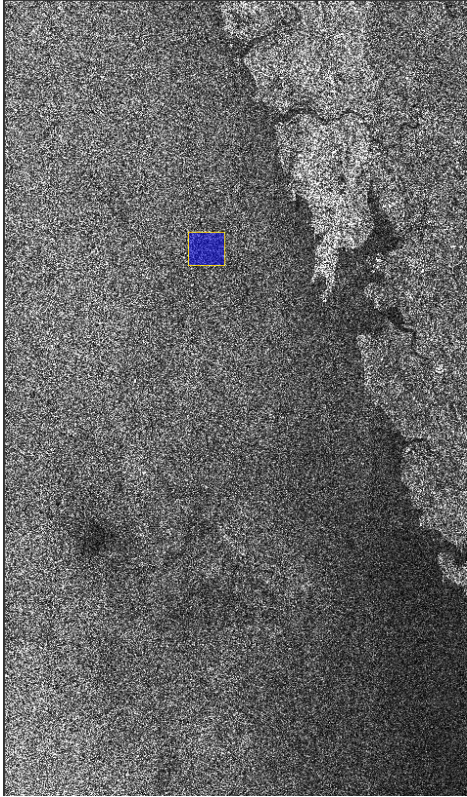


Fig.12. The SAR image was acquired by the ICEYE-X6 satellite on 24 June 2022 during night time, covering an area of 20,000 sqkm along the coastline of Maharashtra, India.

The SAR image^[22] shown in Fig.12 was acquired by the ICEYE-X6 satellite on 24 June 2022 during night time, which operates on X-band, in Scan mode, VV polarization, covering an area of 20,000 sqkm along the coastline of Maharashtra, India. The data format was Ground Range Detected (GRD) in GeoTiff format and the image has a resolution better than 15m.

The SAR image #2 shown in Fig.13 is a slice (marked in blue rectangular) cut from the SAR dataset shown in Fig.12. The SAR image #2 is of size 1455×1707 and 6 ships are visible. The sea waves make the SAR background look rough.

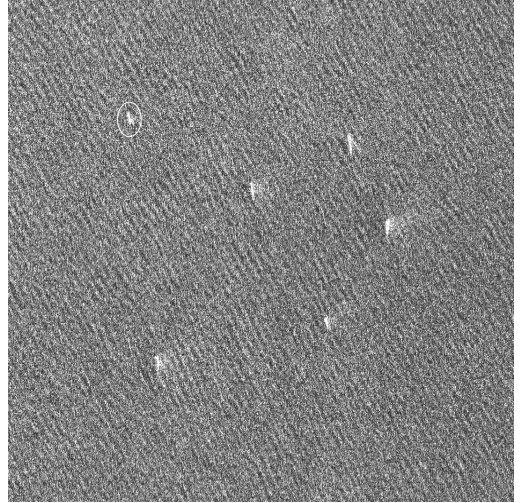


Fig.13. The SAR image #2 from ICEYE.

The statistical analysis of the SAR image #2 is given in Fig.14. Similarly, the pixels of 6 ships body in Fig.13 are discarded from the SAR image before a statistical distribution fitting is carried out. The histogram of pixels of the clutter background in SAR image #2 is given in Fig.14, and the PDF curves of Gaussian, Weibull, K and Gamma distributions to fit the background clutter data are also included. Also, the tails of statistical distribution of the SAR image #2 is given in Fig.15. Different from the SAR image #1, it can be seen that both the main body and tail of the PDF of K distribution fit the histogram of the SAR image #2 very well, and that of the Gaussian greatly deviate from the histogram of the SAR image #2 as expected. The tail of the Weibull distribution is slightly lower than that of the histogram of the SAR image #2, and the tails of the PDF of both Gamma distributions are higher than that of the histogram of the SAR image #2 at some degree. We can see that the goodness of fit for these statistical distributions to the SAR image #2 is different from the situation of the SAR image #1.

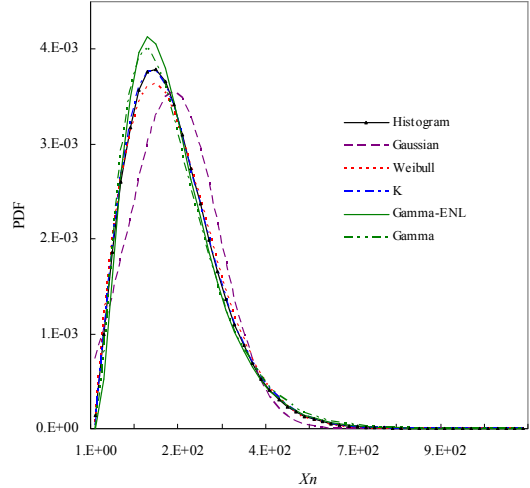


Fig.14. The analysis of statistical distribution on the SAR image #2.

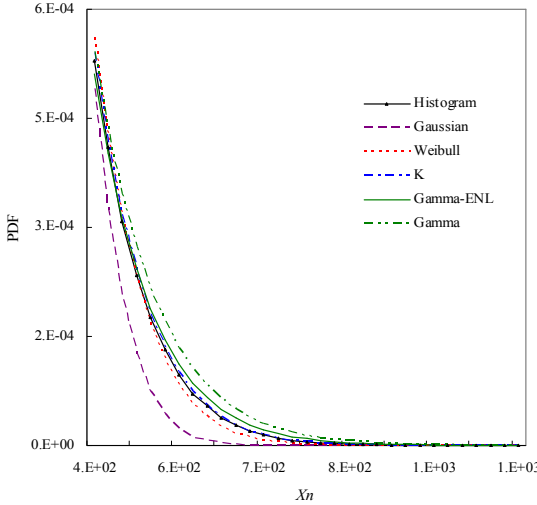
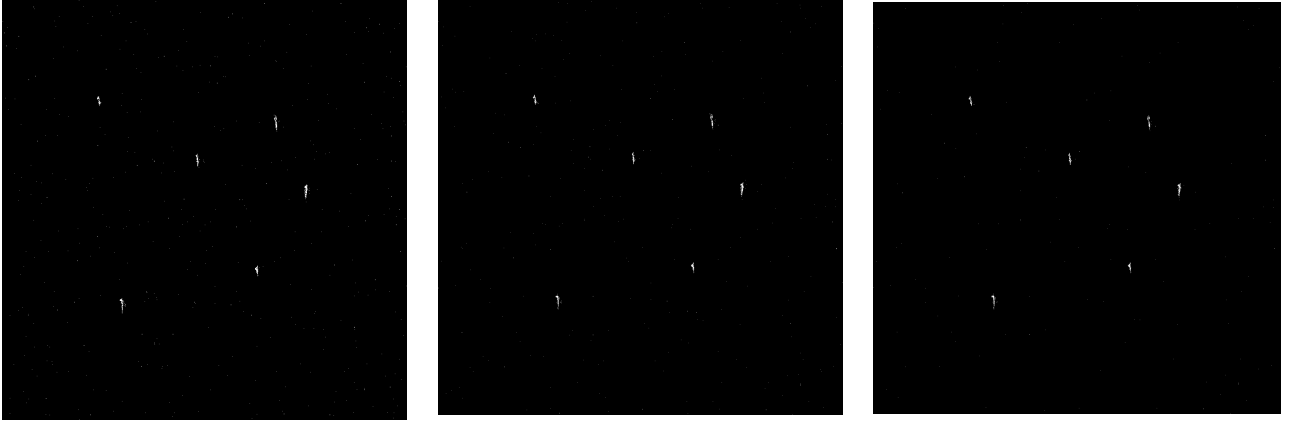


Fig.15. The tails of statistical distribution of the SAR image #2.

2) The performance analysis of the Wilcoxon nonparametric detector

Here, the Wilcoxon nonparametric detector takes a test window of size $t \times t=2 \times 2$, three boundary rows/columns $q=3$ of reference samples, a width $g=60$ of the guard area, and the total number of the reference samples is 1500. The two-parameter CFAR, the Weibull CFAR and the TS-CFAR take a single pixel in the test window, a single boundary row/column $q=1$ of reference samples, and a same width $g=60$ of the guard area. The total number of the reference samples is 488 for them. For the TS-CFAR scheme, the truncation ratio is $R_t=10\%$.

The detection result of the two-parameter CFAR on the SAR image #2 is shown in Fig.16 (a), (b) and (c) for the nominal false alarm rate $P_{fa}=10^{-6}$, 10^{-7} and 10^{-8} ,



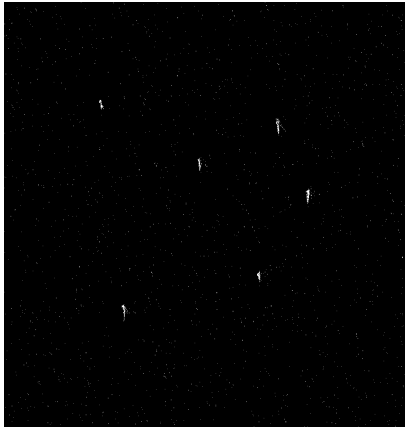
(a) $P_{fa}=10^{-6}$, FDR \$\approx\$ - . (b) $P_{fa}=10^{-7}$, FDR \$\approx\$ - . (c) $P_{fa}=10^{-8}$, FDR \$\approx 0.95\$.

Fig.16. The detection results of the two-parameter CFAR on the SAR image #2.

respectively. The detection result of the Weibull CFAR on the SAR image #2 is given in Fig.17 (a), (b) and (c) for the nominal false alarm rate $P_{fa}=10^{-3}$, 10^{-4} and 10^{-5} , respectively. The detection result of the TS-CFAR on the SAR image #2 is shown in Fig.18 (a), (b) and (c) for the nominal false alarm rate $P_{fa}=10^{-2}$, 10^{-3} and 5×10^{-4} , respectively. The detection result of the Wilcoxon CFAR on the SAR image #2 at the nominal false alarm rate $P_{fa}=10^{-6}$, 10^{-7} and 10^{-8} is given in Fig.19 (a), (b) and (c), respectively.

It can be seen that when the SAR detection scene changes from the SAR image #1 to the SAR image #2, the nominal false alarm rate of the Wilcoxon nonparametric CFAR in Fig.19(c) is the same $P_{fa}=10^{-8}$ as in Fig.9(c), the false alarm performance of the Wilcoxon nonparametric CFAR can still maintain an acceptable level. This is due to the fact that the false alarm rate of the Wilcoxon nonparametric CFAR is irrelevant to the distribution of background clutter. The FDR in Fig.16(c), that in Fig.17(c), that in Fig.18(c) and that in Fig.19(c) are very close. This means that the false alarm performance for the detection result by the two-parameter CFAR in Fig.16(c), that by the Weibull CFAR in Fig.17(c), that by the TS-CFAR in Fig.18(c) and that by the Wilcoxon nonparametric CFAR in Fig.19(c) are similar. Nevertheless, the nominal false alarm rate of the two-parameter CFAR, the Weibull CFAR, the TS-CFAR and the Wilcoxon nonparametric CFAR are different here.

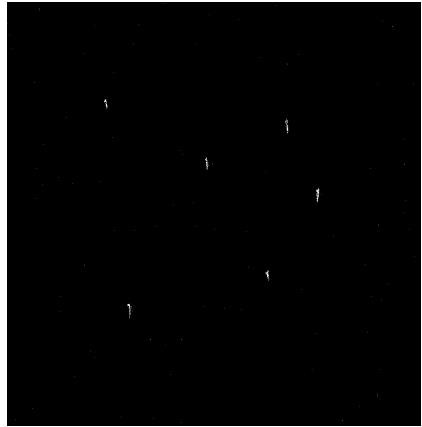
The detection effect on a single ship (in the white circle) in the SAR image #2 by the two-parameter CFAR in Fig.16(c), the Weibull CFAR in Fig.17(c), the TS-CFAR in Fig.18(c) and the Wilcoxon nonparametric CFAR in Fig.19(c) is shown in Fig.20 again. The suppression effect on sidelobe of ship by the Wilcoxon nonparametric CFAR is also observed here.



(a) $P_{\text{fa}}=10^{-3}$, FDR≈--



(b) $P_{\text{fa}}=10^{-4}$, FDR≈--



(c) $P_{\text{fa}}=10^{-5}$, FDR≈0.94

Fig.17. The detection results of the Weibull CFAR on the SAR image #2.



(a) $P_{\text{fa}}=10^{-2}$, FDR≈--



(b) $P_{\text{fa}}=10^{-3}$, FDR≈--



(c) $P_{\text{fa}}=5 \times 10^{-4}$, FDR≈0.95

Fig.18. The detection results of the TS-CFAR scheme on the SAR image #2.



(a) $P_{\text{fa}}=10^{-6}$, FDR≈--



(b) $P_{\text{fa}}=10^{-7}$, FDR≈--



(c) $P_{\text{fa}}=10^{-8}$, FDR≈0.94

Fig.19. The detection results of the Wilcoxon nonparametric detector on the SAR image #2

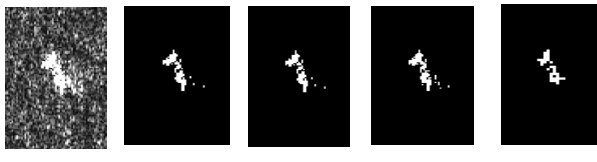


Fig.20. The detection effects of several detectors on ship in the SAR image #2.

3) The time cost of the Wilcoxon nonparametric detector

The execution times of the two-parameter CFAR, the Weibull CFAR, the TS-CFAR and the Wilcoxon nonparametric detector on the SAR image #2 are given in Table II, respectively. It's shown that among these CFAR schemes the ship detection on the SAR image #2 by the Wilcoxon nonparametric detector is the fastest, and it reduces nearly half of execution time of the two-parameter CFAR. The execution time of the TS-CFAR is the longest. This is similar to the result on the SAR image #1.

TABLE II

The execution times of several CFAR detectors on the SAR image #2

| TP-CFAR | Weibull | TS-CFAR | Wilcoxon |
|---------|---------|----------|----------|
| 101.54s | 946.88s | 2578.96s | 55.25s |

C. The weak ship detection in rough SAR background.

1) The SAR Image #3 collected by Gaofen-3

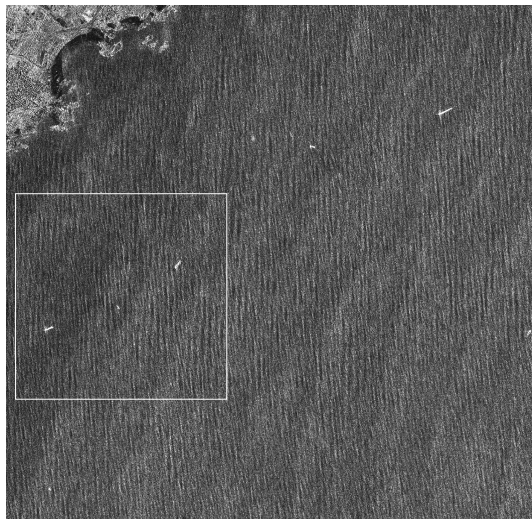


Fig.21 The SAR image is a scene of the AIR-SARShip-1.0 dataset acquired by the C-band Gaofen-3.

The SAR image shown in Fig.21 is a scene of the AIR-SARShip-1.0 dataset^[23]. The AIR-SARShip-1.0 dataset is collected by the Gaofen-3 satellite, which is the first Chinese C-band multi-polarization high-resolution synthetic aperture radar satellite. The image has a resolution of 3m, in a single polarization mode, and saved in the “tiff” format. The SAR image #3 shown in Fig.22 is a slice (marked in white rectangular) cut from the SAR scene shown in Fig.21. The SAR image #3 is of size 1201×1101. There are 2 obvious

ships and a weak ship (in a red circle) in the SAR image #3. The sea condition is Level 4, the ripples caused by the waves are clearly visible.

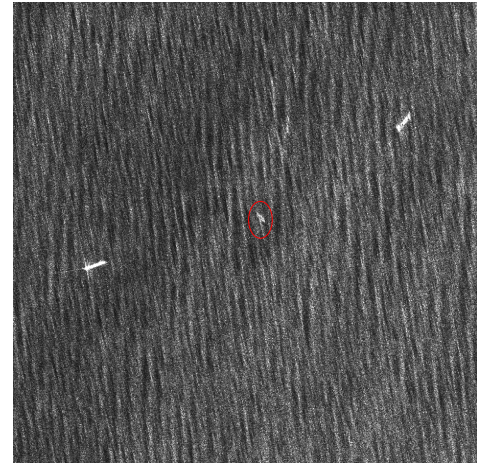


Fig.22 The SAR image #3 from Gaofen-3.

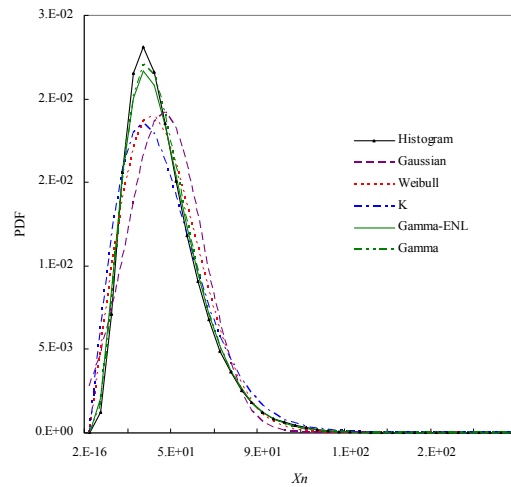


Fig.23. The analysis of statistical distribution on the SAR image #3.

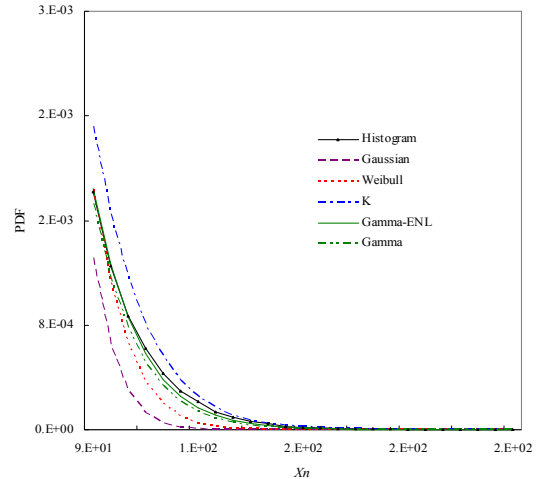


Fig.24. The tails of statistical distribution of the SAR image #3.

In order to model the statistical distribution of the SAR image #3, the ships in the SAR image are discarded as before.

The statistical analysis of the SAR image #3 is presented in Fig.23. The tails of the statistical distribution of the SAR image #3 is illustrated in Fig.24. It can be seen that the situation of the statistical distribution fitting for the SAR image #3 differ from the former both cases. None of these distribution models fits the histogram of the SAR image #3 very well. For the tails of the distribution, the closest to the tails of histogram for the SAR image #3 is that of the Gamma distribution with ENL, that of Gamma by the maximum likelihood method is slightly lower than it, and that of Weibull is even lower. The tail of Gaussian deviate greatly from the tails of histogram for the SAR image #3, and the tail of K distribution is slightly higher than it. Therefore, a specific statistical distribution may fits a certain SAR scene well, but if the SAR detection scene turns a different one, the assumed distribution may deviate from the actual SAR background such that the false alarm performance of a parametric CFAR scheme may deteriorate. Since the false alarm rate of Wilcoxon nonparametric CFAR is irrelative to the distribution type of the SAR background. This is the main motivation for us to apply the Wilcoxon nonparametric CFAR to the ship detection in SAR images.

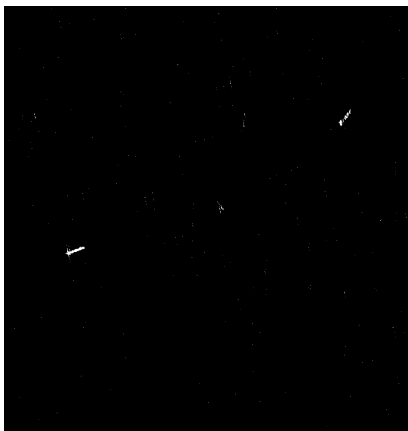
2) The performance analysis of the Wilcoxon nonparametric detector

Here we shall verify the detection effect of the Wilcoxon nonparametric CFAR on the weak ship in rough sea surface shown in the SAR image #3. The two-parameter CFAR, the Weibull CFAR and the TS-CFAR take a single pixel in the test window, a single boundary row/column $q=1$ of reference samples, and a width $g=60$ of the guard area. The total number of the reference samples is 488 for them. For the TS-CFAR scheme, the truncation ratio is also $R_t = 10\%$. The Wilcoxon nonparametric detector takes a test window of size $t \times t=2 \times 2$, three boundary rows/columns $q=3$ of reference samples, a width $g=60$ of the guard area, and the total number of the reference samples is 1500. In order to detect more details of the weak ship body, the Wilcoxon nonparametric CFAR slides a pixel for each of detection here.

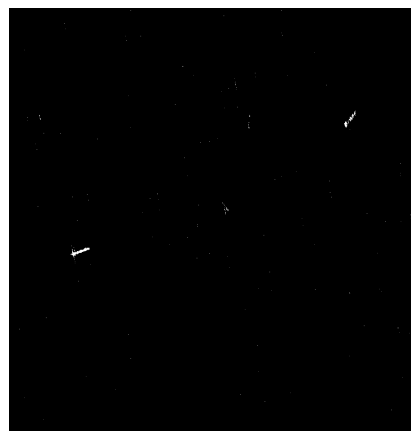
The detection result of the two-parameter CFAR on the SAR image #3 is shown in Fig.25 (a), (b) and (c) for the nominal false alarm rate $P_{fa}=10^{-9}$, 10^{-10} and 10^{-11} , respectively. The detection result of the Weibull CFAR on the SAR image #3 is shown in Fig.26 (a), (b) and (c) for the design false alarm rate $P_{fa}=10^{-6}$, 10^{-7} and 5×10^{-8} , respectively. The detection result of the TS-CFAR on the SAR image #3 is shown in Fig.27 (a), (b) and (c) for the design false alarm rate $P_{fa}=10^{-3}$, 10^{-4} and 3×10^{-5} , respectively. The detection result of the Wilcoxon detector on the SAR image #3 at the design false alarm rate $P_{fa}=10^{-6}$, 10^{-7} and 10^{-8} is shown in Fig.28 (a), (b) and (c), respectively. The FDR in Fig.25(c), that in Fig.26(c), that in Fig.27(c) and that in Fig.28(c) are very close. This means that the false alarm performance for the detection result by the two-parameter detector in Fig.25(c), that by the Weibull-CFAR in Fig.26(c), that by the TS-CFAR in Fig.27(c) and that by the Wilcoxon nonparametric CFAR in Fig.28(c) are similar.

For the detection results of the Wilcoxon nonparametric CFAR on the SAR image #1, #2 and #3 shown in Fig.9(c), Fig.19(c) and Fig.28(c), the nominal false alarm rate is always set at $P_{fa}=10^{-8}$, but the Wilcoxon nonparametric CFAR can obtain an acceptable false alarm performance. This is due to the advantage of Wilcoxon nonparametric that its false alarm rate is irrelative to the distribution type of the SAR background. Therefore, the robustness of the Wilcoxon nonparametric detector to maintain a good false alarm performance in different detection backgrounds is obtained. In order to obtain a similar FDR of the Wilcoxon nonparametric CFAR on the SAR image #1, #2 and #3 at the nominal false alarm rate $P_{fa}=10^{-8}$, the nominal false alarm rate of the two-parameter CFAR for the SAR image #1, #2 and #3 is $P_{fa}=10^{-7}$, $P_{fa}=10^{-8}$ and $P_{fa}=10^{-11}$, respectively. The variation range of the nominal false alarm rate of the two-parameter CFAR is from $P_{fa}=10^{-7}$ to $P_{fa}=10^{-11}$, 4 orders of magnitude. In other words, if the nominal false alarm rate of the two-parameter CFAR is kept the same, the false alarm performance of the two-parameter CFAR in different SAR clutter backgrounds will not maintain constant and the more excessive false alarms will occur. Similarly, in order to make a similar FDR of the Wilcoxon nonparametric CFAR on the SAR image #1, #2 and #3 at the nominal false alarm rate $P_{fa}=10^{-8}$, the nominal false alarm rate of the Weibull CFAR is $P_{fa}=10^{-5}$, $P_{fa}=10^{-5}$ and $P_{fa}=5 \times 10^{-8}$, respectively. The variation range of the nominal false alarm rate of the Weibull CFAR is from $P_{fa}=10^{-5}$ to $P_{fa}=5 \times 10^{-8}$, more than 2 orders of magnitude. In order to reach a similar FDR of the Wilcoxon nonparametric CFAR on the SAR image #1, #2 and #3 at the nominal false alarm rate $P_{fa}=10^{-8}$, the nominal false alarm rate of the TS-CFAR is $P_{fa}=10^{-4}$, $P_{fa}=5 \times 10^{-4}$, and $P_{fa}=3 \times 10^{-5}$, respectively. The variation range of the nominal false alarm rate of the TS-CFAR is from $P_{fa}=5 \times 10^{-4}$ to $P_{fa}=3 \times 10^{-5}$, about 1 order of magnitude. This is due to the fact that the assumed Gaussian, Weibull and Gamma distributions by the two-parameter CFAR, the Weibull CFAR and the TS-CFAR are not consistent with the actual distribution of the SAR image #1, #2 and #3 completely. Among 3 parametric CFAR schemes considered here, the variation range of the nominal false alarm rate of the TS-CFAR is the least. Thus, the ability of the TS-CFAR with assumed Gamma distribution to control the false alarms in different SAR detection environments is relatively strong.

In order to observe the detection effect of the Wilcoxon nonparametric CFAR on the weak ship in the red circle in the SAR image #3, the detection results of these detectors in Fig.25(c), Fig.26(c), Fig.27(c) and Fig.28(c) are illustrated in Fig.29 again. It can be seen that more pixels in the ship body are detected by the Wilcoxon nonparametric detector relative to the two-parameter detector, the Weibull-CFAR and the TS-CFAR. Therefore, the detect performance of the Wilcoxon nonparametric CFAR on the weak ship is improved at some degree.



(a) $P_{fa}=10^{-9}$, FDR≈--



(b) $P_{fa}=10^{-10}$, FDR≈--

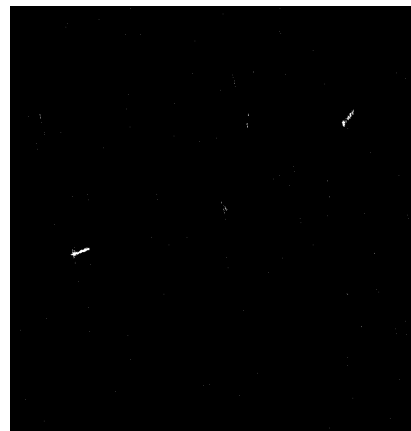


(c) $P_{fa}=10^{-11}$, FDR≈0.97

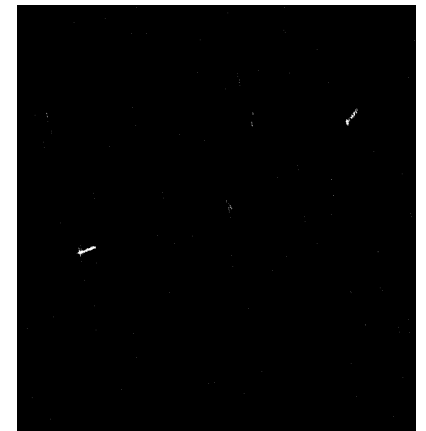
Fig.25. The detection results of the two-parameter CFAR on the SAR image #3



(a) $P_{fa}=10^{-6}$, FDR≈--



(b) $P_{fa}=10^{-7}$, FDR≈--

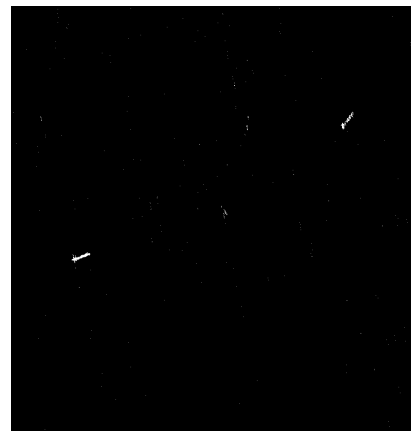


(c) $P_{fa}=5 \times 10^{-8}$, FDR≈0.96

Fig.26. The detection results of the Weibull CFAR on the SAR image #3



(a) $P_{fa}=10^{-3}$, FDR≈--

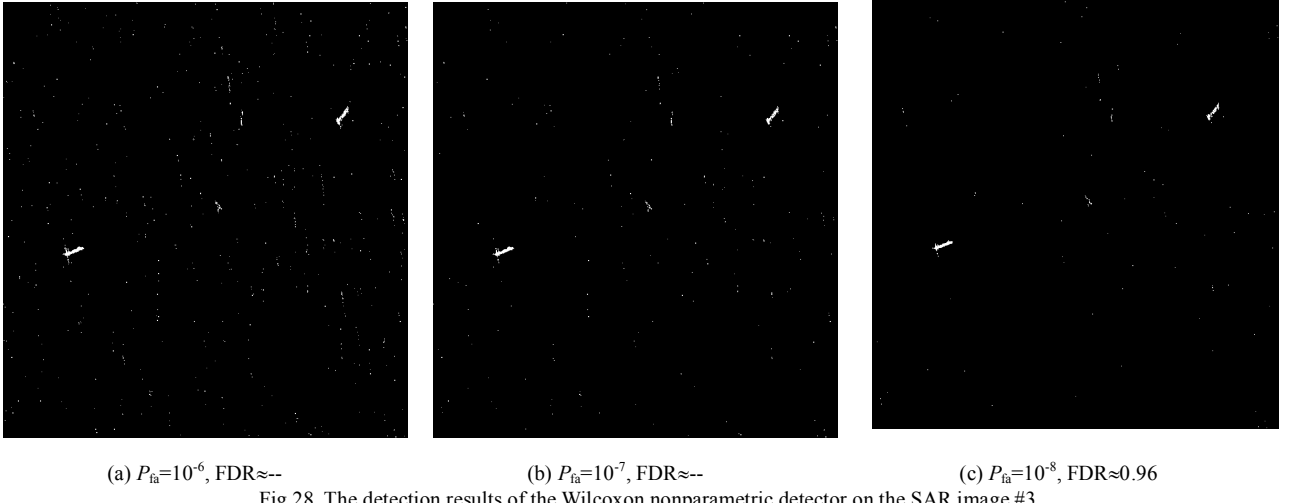


(b) $P_{fa}=10^{-4}$, FDR≈--



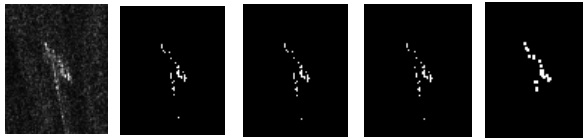
(c) $P_{fa}=3 \times 10^{-5}$, FDR≈0.97

Fig.27. The detection results of the TS-CFAR on the SAR image #3



(a) $P_{fa}=10^{-6}$, FDR≈-- (b) $P_{fa}=10^{-7}$, FDR≈-- (c) $P_{fa}=10^{-8}$, FDR≈0.96

Fig.28. The detection results of the Wilcoxon nonparametric detector on the SAR image #3



(a) ship (b)Gaussian (c)Weibull (d)TS-CFAR (e)Wilcoxin

Fig.29. The detection effects of several detectors on ship in SAR image #3.

3) The time cost of the Wilcoxon nonparametric detector

The execution times of the two-parameter CFAR, the Weibull CFAR, the TS-CFAR and the Wilcoxon nonparametric detector on the SAR image #3 are given in Table III, respectively. It's shown that among these CFAR schemes the time cost of the two-parameter CFAR on the SAR image #3 is the least, and that of Wilcoxon nonparametric CFAR is about 2 times of that of the two-parameter CFAR. This is due to the fact that the Wilcoxon nonparametric CFAR slides one pixel for each of detection in order to detect more details of the weak ship body here, whereas the Wilcoxon nonparametric CFAR slides 2 pixels for each of detection in the cases of the SAR image #1 and the SAR image #2. The time cost of the TS-CFAR is the longest.

TABLE III

The execution times of several CFAR detectors on the SAR image #3

| TP-CFAR | Weibull | TS-CFAR | Wilcoxon |
|---------|---------|----------|----------|
| 42.45s | 468.37s | 1343.88s | 118.62s |

IV. CONCLUSION

The ship detection in SAR images becomes a hot topic in the field of marine remote sensing, and a lot of papers focused on this problem have been published in the past. Most of them belong to the parametric CFAR detection schemes which assume a known clutter distribution for SAR image background. The parametric CFAR detector suffers from the disadvantage that the detection threshold is sensitive to changes of the background clutter

distribution. Even if the distribution of the clutter data is known at some time, uncontrollable phenomena may cause changes such that at a later time the clutter distribution is vastly different. Because the nonparametric CFAR detector has an inherent advantage that it can maintain a constant false alarm rate even if the clutter distribution becomes a different one. The Wilcoxon nonparametric CFAR scheme for the ship detection in SAR image is proposed and analyzed in this work. A closed form of the false alarm rate for the Wilcoxon nonparametric CFAR detector to determine the decision threshold is presented. The comparison between the detection performance of the Wilcoxon nonparametric detector, that of the two-parameter CFAR, that of the Weibull CFAR and that of the TS-CFAR is made, and our experimental tests are carried out on Radarsat-2, ICEYE-X6 and Gaofen-3 SAR images.

It is shown that for a specific SAR detection scene, the two-parameter CFAR detector at a lower design P_{fa} can achieve a similar detection effect of the Weibull CFAR scheme. This is due to the fact that the two-parameter CFAR assumes a Gaussian distribution for the background clutter, whereas the actual clutter in SAR image obeys a nonGaussian distribution with a long tail. Therefore, a higher detection threshold corresponding to a lower design P_{fa} is required for the two-parameter CFAR to suppress the excessive false alarms from the background clutter. This may be the main cause by it that the two-parameter CFAR can find a wide application in the SAR image target detection field. Therefore, the comparison of the detection performance between the detectors with different assumed distributions under the same nominal/design false alarm rate P_{fa} is unfair. From a new point of view that under an equal or similar FDR for a specific SAR image, the comparison of the detection performance of different CFAR detectors will be of more practical importance. However, the clutter background in SAR images is complicated and variable. When the SAR detection scene becomes a different one, the false alarm performance of the two-parameter CFAR with the same design false alarm

rate will deteriorate greatly.

It's shown that if the nominal false alarm rate of the Wilcoxon nonparametric CFAR is set at $P_{fa}=10^{-8}$, the Wilcoxon nonparametric CFAR can obtain an acceptable false alarm performance for the detection results on the SAR image #1, #2 and #3. However, in order to obtain a similar false alarm performance for the Wilcoxon nonparametric CFAR, the nominal false alarm rate of the two-parameter CFAR, the Weibull CFAR and the TS-CFAR on the SAR image #1, #2 and #3 varies 4 orders of magnitude, 2 orders of magnitude and 1 order of magnitude, respectively. This is due to the fact that the false alarm rate of Wilcoxon nonparametric CFAR is irrelative to the distribution type of the SAR background. Therefore, the false alarm performance of the Wilcoxon nonparametric CFAR is robust to these different backgrounds. Among 3 parametric CFAR schemes considered here: the two-parameter CFAR, the Weibull CFAR and the TS-CFAR, the ability of the TS-CFAR with assumed Gamma distribution to control the false alarms in different SAR detection environments is relatively strong, but its execution time is too long.

Moreover, the Wilcoxon nonparametric detector can suppress the false alarms resulting from the sidelobes to some extend, relative to the two-parameter CFAR, the Weibull CFAR and the TS-CFAR. Also, the detection performance of the Wilcoxon nonparametric CFAR on the weak ship is improved at some degree. The detection speed of the Wilcoxon nonparametric detector is fast, and it saves nearly half of execution time of the two-parameter CFAR. The Wilcoxon nonparametric detector needs only $m \times n + 1$ comparators and an accumulator to be implemented, thus it has the simplicity of hardware implementation. Since the Wilcoxon nonparametric detector does not assume a known distribution for the background clutter, it avoids the complexity and the large computation time of the maximum likelihood estimation on the distribution parameters for the parametric CFAR detector. Therefore, the Wilcoxon detector can be a good choice of the ship detection technique in the SAR image.

In order to enhance the robustness of the detection performance of the Wilcoxon nonparametric detector in nonhomogeneous background caused by multiple targets and clutter boundaries, the Wilcoxon nonparametric detector will be integrated with the adaptive censoring technique, such as the ordered data variable (ODV)^[24], adaptive truncated statistics (ATS)^[8], etc, with the sub-window selection methods, such as the greatest of (GO), the smallest of (SO) and the variable index (VI) CFAR^[25], along with the superpixel-level technique^[26,27] to propose some modified Wilcoxon nonparametric detector for nonhomogeneous background. We shall accomplish these tasks in the near future.

ACKNOWLEDGMENT

I would like to express my thanks to the ICEYE sample dataset^[22], High-resolution SAR Ship Detection Dataset:

AIR-SARShip-1.0^[23] and Prof. Liu Hongwei with Xidian University for the helps on our experimental SAR images. This work is supported by the National Natural Science Foundation of China under Grant No. 62171402 and No.61179016.

REFERENCES

- [1] L. M. Novak, G. J. Owirka, and C. M. Netishen, "Performance of a high-resolution polarimetric SAR automatic target recognition system," Lincoln Lab. J., vol.6, no.1, pp.11-24, 1993.
- [2] P. Lombardo and M. Sciotti, "Segmentation-based technique for ship detection in SAR images," IEE Proc. Radar, Sonar Navig., vol.148, no.3, pp.147-159, Jun. 2001.
- [3] M. S. Liao, C. C. Wang, Y. Wang, and L. M. Jiang, "Using SAR images to detect ships from sea clutter," IEEE Geosci. Remote Sens. Lett., vol.5, no. 2, pp.194-198, Apr. 2008.
- [4] G. Gao, L. Liu, L. J. Zhao, G. T. Shi, and G. Y. Kuang, "An adaptive and fast CFAR algorithm based on automatic censoring for target detection in high-resolution SAR images," IEEE Trans. on Geosci. Remote Sens., vol.47, no.6, pp. 1685-1697, Jun. 2009.
- [5] B. Hou, X. Z. Chen, and L. C. Jiao, "Multilayer CFAR detection of ship targets in very high resolution SAR images," IEEE Geosci. Remote Sens. Lett., vol.12, no.4, pp.811-815, Apr. 2015.
- [6] D. Tao, S. N. Anfinsen, and C. Brekke, "Robust CFAR detector based on truncated statistics in multiple target situations," IEEE Trans. on Geosci. Remote Sens., vol.54, no.1, pp.117-134, Jan. 2016.
- [7] F. Nar, O. E. Okman, A. Ozgur, and M. Cetin, "Fast target detection in radar images using Rayleigh mixtures and summed area tables," Digit. Signal Process., vol.77, pp.86-101, 2018.
- [8] J. Q. Ai, Q. W. Luo, X. Z. Yang, Z. P. Yin, and H. Xu, "Outliers-robust CFAR detector of Gaussian clutter based on the truncated-maximum-likelihood-estimator in SAR imagery," IEEE Trans. on Intelligent Transportation Syst., vol.21, no.5, pp.2039-2049, May 2020.
- [9] R.G. Zefreh, M.R. Taban, M.M. Naghsh, and S. Gazor, "Robust CFAR detector based on censored harmonic averaging in heterogeneous clutter," IEEE Trans. Aerosp. Electron. Syst., vol.57, no.3, pp.1956-1963, Jun. 2021.
- [10] J. Q. Ai, Y. X. Mao, Q. W. Luo, M. D. Xing, K. Jiang, and X. M. Yang, "Robust CFAR ship detector based on bilateral-trimmed-statistics of complex ocean scenes in SAR imagery: a closed-form solution," IEEE Trans. Aerosp. Electron. Syst., vol.57, no.3, pp.1872-1890, Jun. 2021.
- [11] J.Q. Ai, Z.L. Pei, B.D. Yao, Z.C. Wang, and M.D. Xing, "AIS data aided Rayleigh CFAR ship detection algorithm of multiple-target environment in SAR images," IEEE Trans. Aerosp. Electron. Syst., vol.58, no.2, pp.1266-1282, Apr. 2022.
- [12] G. W. Zeoli and T. S. Fong, "Performance of a two-sample Mann-Whitney nonparametric detector in

- a radar application," IEEE Trans. Aerosp. Electron. Syst., vol.7, no.5, pp.951–959, Sep. 1971.
- [13] V. G. Hansen and B. A. Olsen, "Nonparametric radar extraction using a generalized sign test," IEEE Trans. Aerosp. Electron. Syst., vol.7, no.5, pp.942–950, Sep. 1971.
- [14] M. Sekine and Y. H. Mao. Weibull Radar Clutter. London: Peter Peregrinus Ltd., 1990.
- [15] G. M. Dillard and C. E. Antoniak, "A practical distribution-free detection procedure for multiple-range-bin radars," IEEE Trans. Aerosp. Electron. Syst., vol.6, no.5, pp.629–635. Sep. 1970.
- [16] X. W. Meng, "Rank sum nonparametric CFAR detector in nonhomogeneous background," IEEE Trans. Aerosp. Electron. Syst., vol.57, no.1, pp.397-403, Feb. 2021.
- [17] X. W. Meng, "Performance evaluation of RQ non-parametric CFAR detector in multiple target and non-uniform clutter," IET Radar Sonar Navig., vol.14, no.3, pp.415-424, 2020.
- [18] J. Hajek, Z. Sidak, and P. K. Sen, Theory of Rank Tests (2nd edn.). Now York: Academic Press, Inc., 1999.
- [19] P. H. Kvam and B. Vidakovic. Nonparametric Statistics with Applications to Science and Engineering. New Jersey: John Wiley & Sons Inc., 2007.
- [20] R. Ravid and N. Levanon, "Maximum-likelihood CFAR for Weibull background," IEE Proc. F, Radar & Signal process., vol.139, no.3, pp.256-264, Jun. 1992.
- [21] P. Ray and P. K. Varshney, "A false discovery rate based detector for detection of targets in clutter and noise," In Proc. IEEE Radar Conference, Rome, Italy, May 26-30, 2008, pp.1-6.
- [22] <https://www.iceye.com/downloads/datasets>.
- [23] X. Sun, Z. R. Wang, Y. R. Sun, W. H. Diao, Y. Zhang, and K. Fu. "AIR-SARShip-1.0: High-resolution SAR Ship Detection Dataset," Journal of Radars, vol.8, no.6, pp.852-863, Dec. 2019.
- [24] A. Farrouki and M. Barkat, "Automatic censoring CFAR detector based on ordered data variability for nonhomogeneous environments," IEE Proc.-Radar Sonar Navig., vol.152, no.1, pp.43-51, Feb. 2005.
- [25] M. E. Smith and P. K. Varshney, "Intelligent CFAR processor based on data variability," IEEE Trans. Aerosp. Electron. Syst., vol.36, no.3, pp.837-847, July 2000.
- [26] W. Y. Yu, Y. H. Wang, H. W. Liu, and J. L. He, "Superpixel based CFAR target detection for high resolution SAR images," IEEE Geosci. Remote Sens. Lett., vol.13, no.5, pp.730–734, May 2016.
- [27] O. Pappas, A. Achim, and D. Bull, "Superpixel level CFAR detectors for ship detection in SAR imagery," IEEE Geosci. Remote Sens. Lett., vol.15, no.9, pp.1397-1401, Sep. 2018.



Xiangwei Meng was born in China in 1966. He graduated from Dalian University of Technology in 1987. He currently serves as a professor at Yantai Nanshan University. He is a member of IET and a senior member of CIE. He acts as a reviewer for *IEEE Trans. on AES*, *IET RSN*, *Signal Processing and Electronics Letters*. His research interests include radar CFAR detection and signal theory.